PROCESS CHAIN FOR NUMERICAL SIMULATION OF IMLS

G. Branner*, G. Strasser*, M. F. Zaeh*
*Institute for Machine Tools and Industrial Management (*iwb*),
Technische Universitaet Muenchen, Germany

Abstract   **Reviewed, accepted September 5, 2007**

Additive layer manufacturing methods imply, among other advantages, extensive flexibility concerning their ability to realize mass customization. Despite various efforts towards process enhancement, numerous deficiencies concerning part distortion or residual stresses are still observable. The present work deals with the definition of an efficient process chain for numerical simulation of indirect metal laser sintering (IMLS), in order to improve dimensional accuracy. The underlying method is based on investigations of dilatometric behavior of iron based powder, which is integrated into reaction kinetic models and coupled with a finite element analysis (FEA). Thus, singular process steps, e. g. solid phase sintering, phase transformations or infiltration, are numerically modelled with adequate accuracy. Referring to thermomechanical simulation, possibilities for pre-scaling of part geometries are presented.

Introduction

In the area of production technology innovative processes to realize complex customized parts are claimed by the industry. Conventional and mostly well known machining production techniques do not have adequate ability to fulfill the changing requirements, which result in growing complexity in conjunction with a high level of integrated functionality [1]. Research facilities work together with industry on the development and optimization of new additive manufacturing processes using metal. In recent years especially technologies based on a direct additive layer manufacturing underlie an accelerating growth [2]. However, the indirect metal laser sintering (IMLS) process is superior to those working on the selective laser melting (SLM) principle in terms of feasible dimension accuracy, due to a very homogeneous energy contribution into the material [3].

IMLS is a layerwise procedure including two process steps. During selective laser sintering (SLS), a mixture of a polymer and metal powder (Laser Form A6) is fractionally sintered in determinate sections of single layers to a green part by use of a CO_2-laser. The following heat treatment in an oven leads to sintering of the green part, whose structural stability at the beginning solely depends on binding forces of the polymer binder [4]. A temperature course is passed through, which activates the process steps of polymeric binder diffusion, solid phase sintering, infiltration and liquid phase sintering [5]. Thus temperature driven chemical and physical procedures in the material cause transient plastic strains, which substantially reduce the profile and dimensional accuracy of the produced part. Linear or function based scale factors are not sufficient for complex geometries to realize a high level of dimension accuracy, due to plastic distortion [6]. For that reason an integrated process chain based on the finite element method (FEM) is developed, which is used for the simulation of the part distortion during heat treatment. Simulation results are utilized in the process chain to pre-scale the calculated distortion values in individual coordinate directions for an optimized building process via an implemented data interface [7].

Chaining method

The developed process chain is characterized by the implementation of further optimizing algorithms besides an integrated numerical simulation. In particular this aspect affects a method to pre-scale part geometries on the basis of calculated distortions during single process steps.

Initially temperature dependent material properties like thermal conductivity $\lambda(T)$ or specific heat capacity $c_p(T)$ are established using laser-flash-analysis (LFA) and dynamic-difference-calorimetry (DSC) for the following calculation of the transient temperature field. The thermo mechanical simulation targeting the evaluation of occurring plastic distortions is performed on the basis of dilatometric measurements for different heating and cooling cycles. Via transformation into reaction kinetic material models, the dilatometric strain characteristics are gathered in an integral way and could be interpreted by FEM in consideration of the underlying geometry. Thereby an integrated description of plasticizing mechanism during the complete heat treatment could be done. Fig. 1 shows the process chain for the optimization of IMLS regarding the dimensional accuracy. A comparison of the calculated part distortion with the initial geometry of the considered part is subsequently used for pre-scaling.
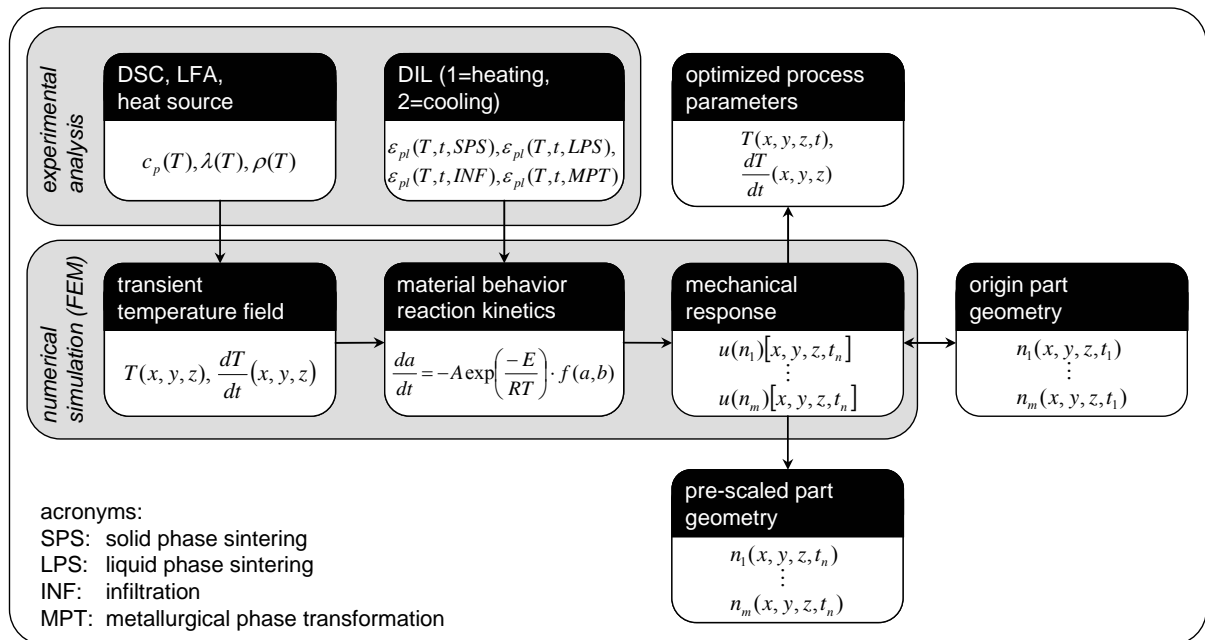

Fig. 1: Process chain implying a numerical simulation method for optimization of dimensional accuracy in IMLS

State of the art

Metal processing and additive production technologies can be fundamentally characterized accordant to the manufacturing principle of layerwise solidification using an energy source. A classification between technologies using the principle of selective laser sintering (SLS) or selective laser melting (SLM) is feasible [8, 9, 10, 11]. To solidify single layers, mechanisms corresponding to fractional or complete melting are distinguished.

In case of the IMLS, solid phase and liquid phase sintering are relevant. During solid phase sintering effects to reduce the energy between single metal particles in terms of diffusion mechanism prevail. Liquid phase sintering is affected by the influence of the bronze alloy. At the infiltration phase of the oven process, first bronze alloy is melted and diffuses into the metal structure later on as a result of capillary pressure [12]. The mechanical strength of the following microstructure is determined by the bonding mechanism between metal and bronze alloy particles in the period of liquid phase sintering [5].

To manufacture parts using the IMLS process, especially materials like LaserForm ST-100 and A6 are relevant. While the powder material LaserForm ST-100 is examined in multiple scientific works regarding powder-metallurgy as well as achievable process reliability [13],

only a few studies exist for the novel material LaserForm A6. Concerning optimization of the surface roughness via laser treatment for example, an extensive examination was done for the material ST-100 [14].

A direct comparison of the commercially available materials ST-100 and A6 is found in [15]. This study presents a well-founded analysis of the powder-metallurgical properties and mechanical strength. Furthermore an overview of the essential process parameters for additive manufacturing and the subsequent heat treatment is given. Due to higher strength of the green part, few advantages regarding the unpacking arise for the material LaserForm A6. In comparison to LaserForm ST-100 less laser power is necessary to solidify single layers, as preheating of the powder material is already possible in the storage containers. DSC measurements suggest a higher melting point at 125.0 °C for LaserForm A6 in comparison to 114.6 °C for LaserForm ST-100. In reference to the manufacturer`s data, the specified strength characteristics of both materials could not be achieved within this analysis. For example measurements result in 283.5 MPa for the yield strength ($R_{p0.2}$) (manufacturer`s data 448.0 MPa, value for ST-100 is 301.0 MPa), 450.5 MPa for the tensile strength (R_m) (735.0 MPa, 586.5 MPa) and 93.7 MPa for Young's modulus (180.0 MPa, 117.0 MPa). Due to larger particle diameters of LaserForm A6, minimal feasible layer thickness increases from 0.05 mm to 0.08 mm. Hence surface quality, in particular for free form surfaces, is reduced as a result of step effects. A modified temperature profile for heat treatment is necessary for the stable processing of LaserForm A6 compared to ST-100.

Characterization of an iron based powder

Thermal material properties

Fundamental input parameters of the integrated process chain for optimization of the dimensional accuracy by means of FEM are temperature dependant material properties for the underlying powder material LaserForm A6. The transient temperature field of thermal simulation, which serves as input for the calculation of the distortion by means of the reaction kinetics, requires in this context characteristic values for the specific heat capacity $c_p(T)$, the thermal conductivity $\lambda(T)$ and the density $\rho(T)$. Due to several sintering steps, this characteristic values have to be evaluated for green part and bronze alloy as well as for the solidified respectively infiltrated material. In case of evaluation of the specific heat capacity the DSC, based on the principle of heat flux, is used. Therefore the specimens are positioned in platinum cups with aluminium oxide inliners and caps under dynamic argon atmosphere (gas flux rate 20 $^{ml}/_{min}$). During the measurement the specimen is heated at a rate of 10 $^{K}/_{min}$ from ambient temperature to 1100 °C. Fig. 2 shows the results of the conducted DSC-evaluation for green part, bronze alloy as well as for combined components during solid phase sintering stating the characteristic temperatures and transformation enthalpies. Furthermore, the specific heat capacity for infiltrated material is displayed.

The measurements for the powder material mixed with polymeric binder show three exothermal peaks at significant temperatures of 164.8 °C, 256.0 °C und 345.9 °C, which characterize single reactions of the binder-diffusion [16]. A complete disruption of the polymeric binder could be noticed at 470.0 °C. Beyond the underlying powder material is labelled by a metallurgical α, γ-transformation with an endothermic enthalpy of 36.31 $^{J}/_{g}$ at 785.0 °C. The analysis of the bronze alloy shows besides the phase-transformation (530.8 °C), the beginning of melting at 790.6 °C and a correlating enthalpy of 151.74 $^{J}/_{g}$. The simulation of solid phase sintering and resulting distortion demands a superposed measurement of powder material and bronze alloy (CuSn10; 85 mass percent). The result of this measurement of powder material combined with bronze alloy is an area characterized by endothermic effects from 800.5 °C to 1086.3 °C. Resulting melting area expansion in comparison to

bronze (777.4 °C – 994.2 °C) is due to penetration of the liquid phase in the porous structure of the solid body as well as alloying. In case of modelling beyond that liquid phase sintering in the numerical simulation, the infiltrated material has to be characterized in detail. In comparison to the proceeding measurements (green part, bronze alloy combined), lower temperatures (609.0 °C) for the creation of the alloy arise.
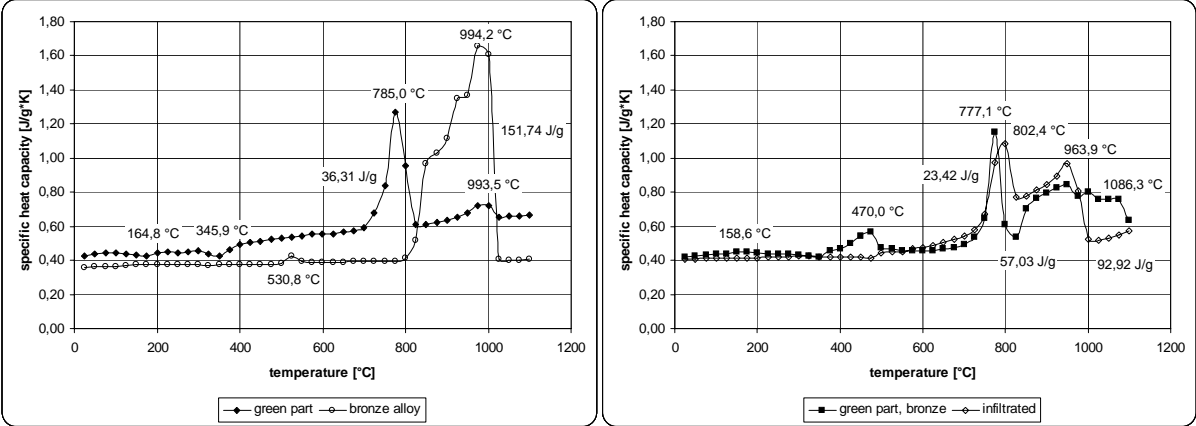

Fig. 2: Specific heat capacity of an iron based powder (green part, bronze alloy, infiltrated part)

Besides specific heat capacity $c_p(T)$, thermal conductivity $\lambda(T)$ is essential for the calculation of the transient temperature field. For the evaluation, initially the thermal diffusivity $a(T)$ has to be identified using the laser flash analysis (LFA). Via multiplication with the density ρ and the specific heat capacity $c_p(T)$, a temperature depending heat conductivity $\lambda(T)$ is calculated:

$$\lambda(T) = \rho \cdot c_p(T) \cdot a(T)$$

A standard specimen holder was used for the LFA measurements. At first specimens without bronze alloy are evaluated while heating and cooling. Afterwards analysis of further specimens with additionally applied bronze alloy (CuSn10; 85 mass percent) are conducted. The resulting values for thermal diffusivity and conductivity of the green part (left hand side) and the infiltrated material (right hand side) are shown in Fig. 3.
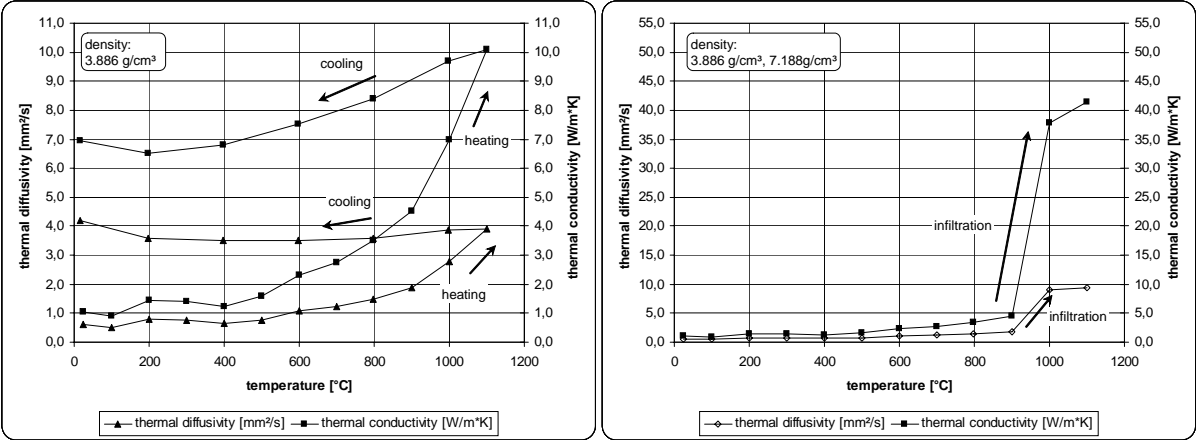

Fig. 3: Thermal diffusivity and conductivity before and after sintering, infiltration

The courses of thermal diffusivity and conductivity (Fig. 3) with significant increases between 100.0 °C and 400.0 °C in the left graphic approve the results of the DSC measurements (disruption of polymeric binder). Beyond a temperature of 900.0 °C the increase of the thermal diffusivity and conductivity amplifies. In case of cooling the graphic shows explicit higher values due to irreversible sintering effects. For the heating of powder material with additional applied bronze (right hand side), beyond 900.0 °C a clear and sharp increase in thermal diffusivity and conductivity is detected. Via infiltration, thermal conductivity rises from 10.1 $^W/_{mK}$ to 41.5 $^W/_{mK}$ (1100.0 °C).

Thermo mechanical material properties

In case of IMLS, a numerical simulation of the 3-dimensional plastic distortional behavior is realized by means of coupling FEM with reaction kinetics. For specific process steps like solid phase sintering, infiltration or liquid phase sintering, the material behavior is integrally characterized by so called reaction kinetic material models. Based on dilatometry, the plastic strains for later heating and cooling periods in the oven cycle are transferred into differential equations. During the measurement, the underlying dilatometer is featured with a fused quartz specimen holder and appropriate mechanical sensors, applying clamping forces between 15 cN and 25 cN. Dilatometry is realized under helium atmosphere (gas-flow-rate 50 $^{ml}/_{min}$). With regard to an efficient process control, temperature is registered using type S thermocouples (Pt/Pt10%Rh) in a range between ambient temperature and 1100.0 °C for characteristic heating rates. Results of thermal dilatation for several powder specimens with defined amount of bronze alloy (CuSn10 for infiltration, 85 mass percent), considering heating rates of 1 $^K/_{min}$, 5 $^K/_{min}$ and 10 $^K/_{min}$, are shown in Fig. 4. Linear thermal expansion of single measurements only differs marginally between 20.0 °C and 720.0 °C. Considering the heating rate of 10 $^K/_{min}$, the metallurgical phase transformation (α-γ) was found in a temperature range between 717.0 ° und 781.0 °C. Subsequent to lattice transformation effects, significant differences in curve progression are established for specimens with and without additional bronze alloy. In case of samples comprising bronze, the maximum of expansion is detected at 903.0 °C. Reaching 1032.0 °C, the bronze alloy is molten completely and diffused in solid state sintered structure. In case of investigated samples without additional bronze, the maximum of volume expansion is found at 1020.0 °C. For this reason, infiltration yields a short-term shrinkage of about 0.23 %. Further differences in curve progression, compared to heating rates of 5 $^K/_{min}$ and 10 $^K/_{min}$, are observed for samples underlying 1 $^K/_{min}$. In addition to resulting minima and maxima in expansion for characteristic temperatures, two other transformation stages are found in the medium temperature range (552.0 °C and 671.0 °C).

Analogous to dilatometry for heating, corresponding investigations are performed for distortional behavior during cooling. Altogether, the dilatometry describes an efficient method for modeling elastic and plastic strains in all phases of the oven cycle in the IMLS process (solid phase sintering, infiltration, liquid phase sintering, metallurgical phase transformations) by means of reaction kinetic material models. Through integrated material behavior description in the FEA, the inserted software is able to interpolate required data for each specific, time-dependent temperature gradient in underlying process phases.

In order to validate single experimental series, a combined dilatometry for a typical temperature sequence of heat treatment (heating period, two isothermal periods, cooling period) with a total duration of 30 h is realized (cp. Fig. 4 right hand side). Corresponding to single gradients, linear thermal expansion up to a temperature of 720.0 °C is observable. Subsequently, several sintering effects and metallurgical phase transformations lead to transient changes in volume expansion. Particularly, the plastic shrinkage of material during isothermal phases (870.0 °C: -0.031 %, 1070.0 °C: -0.365 %) is of an essential significance.
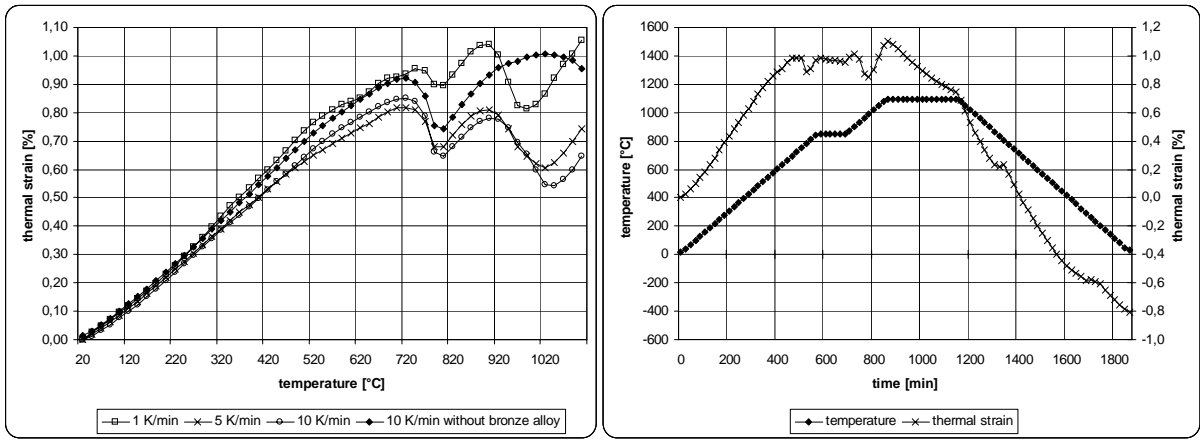
Fig. 4: Thermal strain of underlying powder material for different heating rates (left) and integral strain analysis for a characteristic temperature sequence

Method for Coupling FEA with reaction kinetics

In order to couple reaction kinetics with FEA, the performed dilatometry for investigated heating rates has to be transferred into differential equations by means of adequate mathematical approximation software. Within this software tool, calculation of essential regress values $Y_{cal}(k,j)$ is performed by use of Runge-Kutta 5th degree solving methods with automated optimization of supporting point numbers for computing differential equations (Prince-Diamond method) [17]. The necessary differential equations result from reaction characteristics. For underlying temperatures, no defined course is required. For this reason, isothermal as well as dynamical measurements are able to be combined, what is a special advantage for superposed experimental series. In order to perform solving for user-defined temperature sequences, temperature $T(t)$ is linearly interpolated between two adjacent points:

$$T(t) = (t - t_{i-1}) \cdot \frac{T(t_i) - T(t_{i-1})}{t_i - t_{i-1}}$$

Integration is implemented over the whole effective range (20.0 °C – 1100.0°C) with initial conditions shown in Fig. 5. Contrary, only partitions representing subsequent analysis regions are included for calculation of deviations LSQ through pre-defining of k = start und k = end:

$$LSQ = \sum_{j=1}^{s} \sum_{k=start}^{k=end} w_{j,k} (Y_{j,k} - \hat{Y}_{j,k})^2$$

By means of applying multi-level reaction schema of type t:i,c for transformation of dilatometry into reaction kinetic material models, a sufficient accuracy is realized. Corresponding differential equations and initial conditions for approximation are constituted in Fig. 5**.**
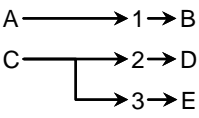
229

reaction scheme	differential equations	initial conditions
t:i,c A ⟶ 1 → B C ⟶ 2 → D ⎣→ 3 → E	$$\frac{da}{dt} = -A_1 \cdot \exp\left(-\frac{E1}{RT}\right) \cdot f1(a,b)$$ $$\frac{db}{dt} = A_1 \cdot \exp\left(-\frac{E1}{RT}\right) \cdot f1(a,b)$$ $$-A_2 \cdot \exp\left(-\frac{E2}{RT}\right) \cdot f2(b,c)$$ $$-A_3 \cdot \exp\left(-\frac{E3}{RT}\right) \cdot f3(b,d)$$ $$\frac{dc}{dt} = A_2 \cdot \exp\left(-\frac{E2}{RT}\right) \cdot f3(b,c)$$	$a = [A]/[A_0]$ $b = [B]/[B_0]$ $c = [C]/[C_0]$ $a_0 = 0.99990$ $b_0 = 0.00008$ $c_0 = 0.00001$

Fig. 5: Differential equations and initial conditions for reaction scheme t:i,c [18]

Within an iterative method, relevant parameters are adjusted as long as experimental dilatometry for heating rates of $1 \, ^K/_{min}$, $5 \, ^K/_{min}$ and $10 \, ^K/_{min}$ fits sufficiently with the description by differential equations. In this context, linear thermal expansion has to be subtracted preliminarily, because reaction kinetics is only able to approximate physical effects based on exponential arrhenius equation [6]. Corresponding reduced plastic dilatometry for defined heating rates is shown in Fig. 6. Beginning with an initial length of 100 %, singular curves indicate a decreasing course resulting from effects like metallurgical phase transformations, solid phase sintering and infiltration. After the completion of heating, samples show a final length of 99.45 % for the rate of $1 \, ^K/_{min}$ and 99.17 % for the rate of $10 \, ^K/_{min}$. Derived reaction kinetic material models for heating and cooling sequences are coupled with FEA. Thus incremental plastic strains representing characteristic phases of heat treatment in the oven process of IMLS are interpolated time and geometry-dependant.
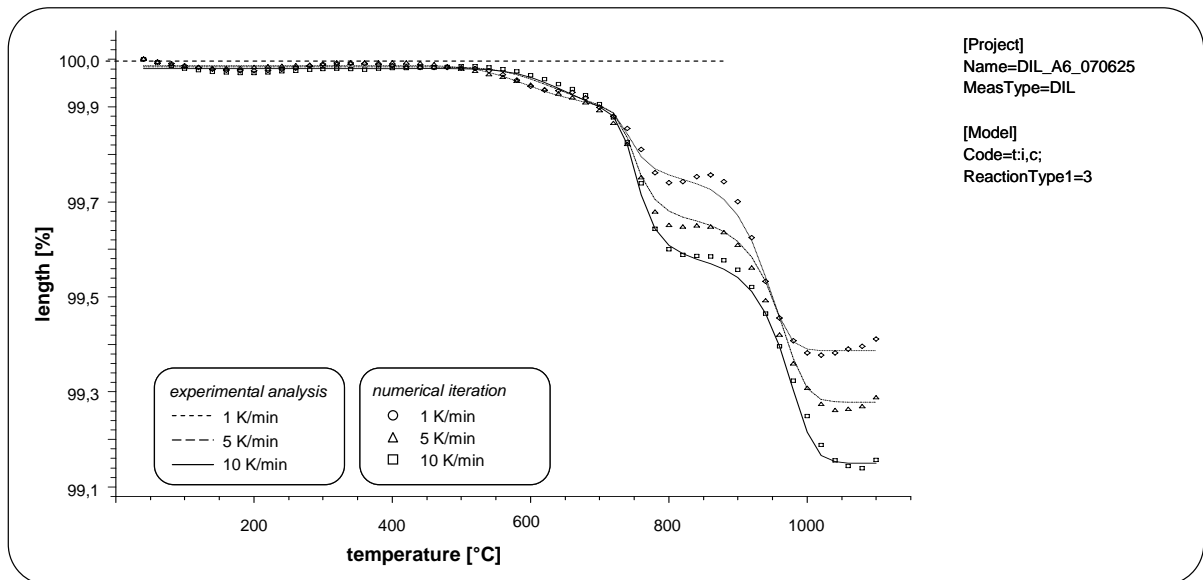

Fig. 6: Nonlinear plastic strain for several heating rates and parameters in the numerical approximation

Results

The presented method provides an opportunity to specify distortional behavior of IMLS part geometries during solid phase sintering, infiltration and liquid phase sintering. Additionally, plastic strains resulting from metallurgical phase transformations are described. However, polymeric binder diffusion in a temperature range between 150.0 °C and 490.0 °C leads to a plastically softening of the whole structure attending gravitational effects. Because softening demonstrates a significant influence on the resulting dimensional accuracy, the mechanisms of polymeric binder diffusion have to be integrated in the underlying process chain. Based on calibration of viscoplastic material models depending on singular specific geometry types, a nonlinear simulation of gravitational effects is performed until reaching a temperature of 500.0 °C. Subsequently, the results are mapped to the initial geometry and the distortional calculation of further process steps is executed on modified part geometry.

In order to demonstrate the potential of the developed method, Fig. 7 shows the meshed geometry of a u-profile with dimensions of 80 mm x 40 mm x 30 mm. Loading the part with gravitation representing the process step of polymeric binder diffusion, a final plastic distortion of 3.31 mm (490.0 °C) in horizontal overhangs is observable in the results of FEA. In case of integrating adequate supports, gravitational effects can be minimized considerably. Corresponding results are mapped to the finite-element mesh for the subsequent numerical simulation of sintering behaviour by means of reaction kinetic material models. Analogous to dilatometry for heating (Fig. 6), a comparable material model in order to describe plastic behavior during cooling is generated and coupled with FEA. By means of coupling calculation of heating and cooling steps resulting dimensional accuracy of parts realized by IMLS can be predicted.
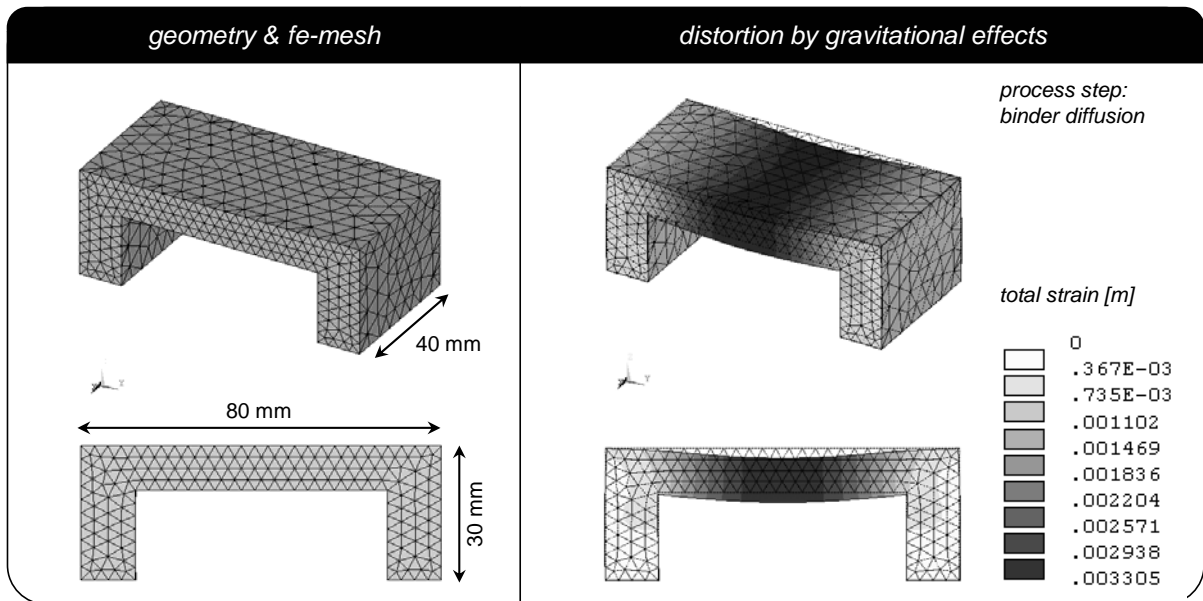

Fig. 7: Meshed u-profile geometry and results of distortion after polymeric binder diffusion

As a result of heat treatment and corresponding physical effects the material comprehends a nonlinear plastic deformation. In order to realize high dimensional accuracy, this deformation has to be compensated through the developed process chain. Fig. 8 shows the final shrinkage of the u-profile resulting at the end of heat treatment. In addition to the distortion of horizontal overhangs by gravitational effects, the structure displays a maximum plastic contraction of about 0.176 mm due to sintering effects. Results of structural calculation are used to compare node coordinates of the warped model with initial node coordinates.

Accordant deviations for each node of the geometry are transformed into the opposite coordinate direction. To include nonlinearities, this so-called pre-scaling of part geometries can be combined with defined scale functions. Subsequent to pre-scaling, a STL data model for selective laser sintering (SLS) is generated.
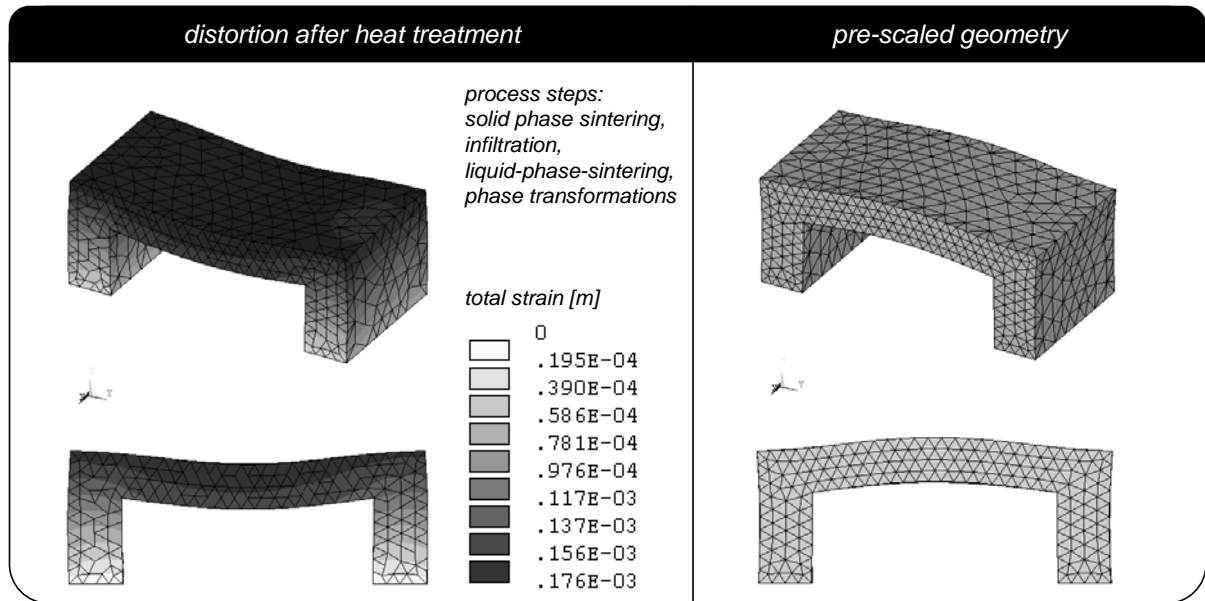

Fig. 8: Results of distortion after heat treatment und pre-scaled u-profile geometry

Conclusions

The developed process chain, based on a FEA, represents an efficient method for the optimization of the dimensional accuracy resulting from heat treatment during IMLS. By means of mathematical approximation of dilatometry for characteristic heating rates through reaction kinetic material models and subsequent coupling with FEM, the distortional behavior in the process steps solid phase sintering, infiltration and liquid phase sintering is predicted. Beyond temperature dependent thermal material properties representing varying physical conditions propagate maximum accuracy for the numerical calculation of 3-dimensional volume distortion by using reaction kinetic material models. Additional influences resulting from gravitational effects in the process step of polymeric binder diffusion are captured through the specific calibration of viscoplastic material models. Due to the pre-scaling of part geometries based on simulation results, the underlying process chain exhibits applicable potential for realizing high dimensional accuracy in IMLS. The developed method can be assigned to further thermal manufacturing processes with negligible effort.

References

[1] Zäh, M. F.; Branner, G.; Hagemann, F.: Chancen und Risiken des Werkzeug- und Formenbaus im globalen Wettbewerb. 3D-Erfahrungsforum: Innovation im Werkzeug- und Formenbau, Munich (2007), pp. 1-1 - 1-15.

[2] Abdel Ghany, K.; Moustafa, S. F.: Comparison between the products of four RPM systems for metals. Rapid Prototyping Journal 12 (2006) 2, pp. 86-94.

[3] Kruth, J. P.; Vandenbroucke, J.; Van Vaerenbergh, J.; Mercelis P.: Benchmarking of different SLS/SLM processes as rapid manufacturing techniques. In.: Int. Conf. Polymers & Moulds Innovations (PMI), Gent, Belgium, April 20-23, 2005.

[4] 3D Systems Corp.: Rapid Tooling, SLA Systems (2006). <http://www.hub-m.com/center/center_file2/002-RapidTooling_delivery.pdf> (02.07.2007).

[5] Kruth, J. P.; Mercelis, P.; Froyen, L.; Rombouts, M.: Binding Mechanisms in Selective Laser Sintering and Selective Laser Melting. Rapid Prototyping Journal 11 (2005) 1, pp. 26-36.

[6] Seefried, M.: Simulation des Prozessschrittes der Wärmebehandlung beim Indirekten-Metall-Lasersintern. Dissertation: Technische Universitaet Muenchen 2005.

[7] Zäh, M. F.; Branner, G.: Optimierung des Indirekten-Metall-Lasersinterns (IMLS) mit Hilfe von neuartigen Simulationsmethoden. 3D-Erfahrungsforum: Innovation im Werkzeug- und Formenbau, Munich (2007), pp. 7-1 - 7-11.

[8] Kruth, J. P.: Material Incress Manufacturing by Rapid Prototyping Techniques. In: CIRP Annals (1991), Vol. 40/2, pp. 603-614.

[9] McAlea, K.; Forderhase, P.; Hejmadi, U.; Nelson, C.: Materials and Applications for the Selective Laser Sintering Process. In: Proc. of the 7th Int. Conf. on Rapid Prototyping, San Francisco (1997), pp. 23-33.

[10] Over, C.; Meiners, W.; Wissenbach, K.; Lindemann, M.; Hutfless, J.: Laser Melting: A New Approach for the Direct Manufacturing of Metal Parts and Tools. In: Proc. Euro-uRapid Int. Users Conf., Frankfurt/Main (2002), A-5.

[11] Levy, G. N.; Schindel, R.; Kruth, J. P.: Rapid Manufacturing and Rapid Tooling with Layer Manufacturing (LM) Technologies, State of the Art and Future Perspectives. In: CIRP Annals (2003), Vol. 52/2, pp. 589-609.

[12] Seefried, M.; Zäh, M. F.: Investigation of the Oven Process in Indirect Metal Laser Sintering. In: Bourell, D. L.; Beaman, J. J.; Crawford, R. H.; Marcus, H. L.; Wood, K. L. (ed.): Solid Freeform Fabrication Proceedings 2004, Austin. Boston (Massachusetts, USA): Kluwer Academic Publisher 2004, pp. 624-635.

[13] Levy, G. N.; Schindel, R.; Schleiss, P.; Micari F.; Fratini, L.: On the use of SLS Tools in Sheet Metal Stamping. CIRP Annals (2003), Vol. 52/1, p. 249 et sqq.

[14] Lamikiz, A.; Sánchez, J.A.; López de Lacalle, L.N.; Arana, J.L.: Laser polishing of parts built up by selective laser sintering. International Journal of Machine Tools and Manufacture (2007).

[15] Levy, G. N.; Schindel, R.; Schleiss, P.: Comparison between LaserForm ST 100 and A6. Rapid 3DSNASUG & SLS Users' Conference (2004).

[16] Seefried, M.; Zäh, M. F.; Meindl, M.: Simulation of the Process Step Polymer Removal in Indirect Metal Laser Sintering. In: Bourell, D. L.; Beaman, J. J.; Crawford, R. H.; Marcus, H. L.; Wood, K. L. (ed.): Solid Freeform Fabrication Proceedings 2004, Austin. Boston (Massachusetts, USA): Kluwer Academic Publisher 2004, pp. 389-399.

[17] Engeln-Müllges, G.; Reuter, F.: Formelsammlung zur numerischen Mathematik mit Turbo Pascal-Programmen. Bibliographisches Institut & F. A. Brockhaus AG, Mannheim 1991, p. 411.

[18] Opfermann, J.: Kinetic Analysis using multivariate non-linear regression. Journal of Thermal Analysis and Calorimetry, Vol. 60 (2000), pp. 641-658.